Supporting Information

Optical temperature sensing with an Er^{3+}, Yb^{3+} co-doped $LaBMoO_6$ single crystal

Xinxu Li,[a] Bingting Bao,[a] Xinyu He,[b] Guoqiang Wang,[a] Yantang Huang,[b] Lingyun Li[a,*] and Yan Yu[a,*]

[a] Key Laboratory of Advanced Materials Technologies, International (HongKong Macao and Taiwan) Joint Laboratory on Advanced Materials Technologies, College of Materials Science and Engineering, Fuzhou University, Fuzhou 350108, China. *lilingyun@fzu.edu.cn, yuyan@fzu.edu.cn*

[b] College of Physics and Information Engineering, Fuzhou University. University Town, Fuzhou 350108, China

Table of Content

1. Synthesis and Characterization of LBMO-PC

1.1 Synthesis and elemental properties of LBMO-PC: Er^{3+}, Yb^{3+}.

Figure S2a show the typical solid state reaction procedure and the sintered LBMO-PC: Er^{3+}, Yb^{3+} tablets, which exhibits bright green emission under 980 nm CW laser excitation. The SEM and EDS images of LBMO-PC: Er^{3+}, Yb^{3+} are shown in **Figure S4**. Except for the grain boundaries and the different particle sizes, the elemental distribution in the LBMO-PC: Er^{3+}, Yb^{3+} is as uniform as that in the LBMO-SC: Er^{3+}, Yb^{3+} crystal. The DRS spectra of LBMO-PC and LBMO-PC: Er^{3+}, Yb^{3+} are shown in **Figure S5**. It can be seen that the absorption edge of the LBMO-PC sample is basically the same as that of the LBMO-SC, and the optical band gap is also 4.3 eV. Meanwhile, LBMO-PC: Er^{3+}, Yb^{3+} has stronger typical absorption peaks than LBMO-SC: Er^{3+}, Yb^{3+}. This is due to the fact that the actual doping ratio of Er^{3+} and Yb^{3+} in the -PC sample is higher than that in the -SC sample, as shown in **Table S3**.

1.2 The influence of sintering temperature and sintering time on the UC properties of LBMO-PC: Er^{3+}, Yb^{3+} powders.

The polycrystalline samples could be successfully synthesized through a wide temperature range. As shown in **Figure S11a**, the PXRD patterns of LBMO-PC: *x*% Er^{3+}, *y*% Yb^{3+} samples sintered at 700, 800, 900 and 1000 ºC match well with the standard one, indicating the successful synthesis of the polycrystalline powders after two rounds of solid state reaction. Although there are few difference in the PXRD patterns, the sintering temperature has obvious influence on the UC fluorescence. As shown in **Figure S11b**, with the increase of sintering temperature, the UC emission intensity increases linearly, and the intensity reaches the highest when the sintering temperature is 1000 ºC. On the other hand, prolonging the sintering time of the second round solid state reaction can also enhance the UC luminescence intensity of the Er^{3+} and Yb^{3+} co-doped LBMO-PC samples. The PXRD patterns of all LBMO-PC: 0.7% Er^{3+}, 10% Yb^{3+} samples sintered at 1000 ºC for 5h, 10h, 12h, 15h and 20h are consistent with that of the standard pattern, as shown in **Figure S12a**. Meanwhile, the UC luminescence intensity of LBMO-PC: 0.7%Er^{3+}, 10%Yb^{3+} sample increases with the prolonging of sintering time from 5h to 15h. But, the prolonging of reaction time can't always enhance the UC luminescence. As shown in **Figure S12b**, the UC emission intensity of LBMO-PC: 0.7% Er^{3+}, 10% Yb^{3+} sample sintered at 1000 ºC for 20h decreases compared with that of the sample sintered for 15h.

1.3 The influence of doping concentration on the UC emission of LBMO-PC: Er^{3+}, Yb^{3+}.

All the UC luminescence spectra of LBMO-PC: Er^{3+}, Yb^{3+} samples shown in **Figure S14** display a typical profile of Er^{3+} emission. All green emission bands are split into three peaks, which is similar to the spectra of LBMO-SC: Er^{3+}, Yb^{3+} as shown in **Figure**

3. The UC luminescence intensity of LBMO-PC: *x*% Er^{3+}, 10% Yb^{3+} and LBMO-PC: 1% Er^{3+}, *y*% Yb^{3+}samples increases with the rising of Er^{3+} and Yb^{3+} content until the maximum intensity is reached when $x = 0.7$ and $y = 10$, respectively. Therefore, the optimum doping concentration of LBMO-PC samples is 0.7% for Er^{3+} and 10% for Yb^{3+}, respectively. The phase of all samples mentioned above is consistent with the standard pattern, as shown in **Figure S13**. In addition, the luminescence decay curve of the $^2H_{11/2}$ state of Er^{3+} was recorded. As shown in **Figure S15**, all luminescence decay curves of LBMO-PC: 0.7% Er^{3+}, *y*% Yb^{3+} samples can also be fitted with first-order exponential functions. The lifetime of LBMO-PC: 0.7% Er^{3+}, *y*% Yb^{3+} samples reaches a maximum value of 133μs at y=12.

1.4 Temperature sensing performance of LBMO-PC: 0.7% Er^{3+}, 10% Yb^{3+} samples sintered at 1000 °C for different time.

Figure S17a and **b** shows the temperature dependent UC luminescence spectra of LBMO-PC: 0.7%Er^{3+}, 10%Yb^{3+} sample sintered at 1000 °C for 5h and 10h. All the luminescence intensities in these figures are normalized based on the luminescence intensities of LBMO-SC: 1%Er^{3+}, 20%Yb^{3+}**.** **Figure S17c** shows the integrated emission intensities of the $^4S_{3/2} \rightarrow {}^4I_{15/2}$ transition displayed for all tested samples in the range of 300 – 500K, the emission intensity of the single crystal sample is always larger than that of all the polycrystalline samples. **Figure S17d** displays the temperature dependent S_a and S_r values of all samples, the S_a and S_r values of all polycrystalline samples are almost the same in the whole measured temperature range. The maximum value of S_r for LBMO-PC:0.7% Er^{3+}, 10% Yb^{3+} samples sintered at 1000 °C for 5h, 10h and 15h are 1.06%, 1.16% and 1.11% at 300K, respectively.

2. Supplementary figures and tables.

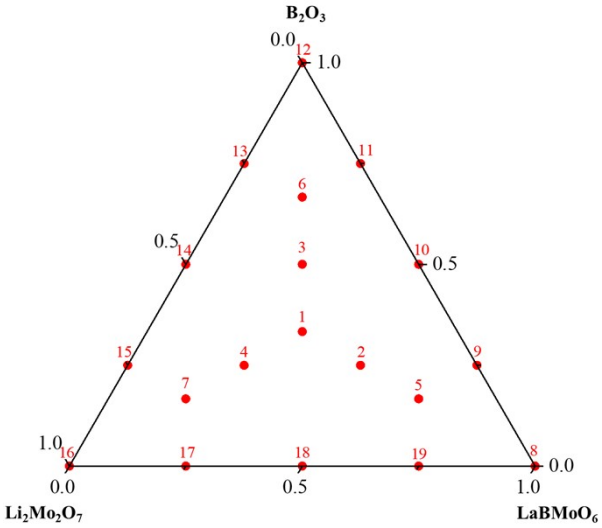

Figure S1. Distribution of flux exploration test points based on mixture design.

Table S1. The composition of test points in Flux exploration experiment (molar ratio)

Test Point	A ($LaBMoO_6$)	B ($Li_2Mo_2O_7$)	C (B_2O_3)
1	0.333333	0.333333	0.333333
2	0.50000	0.25000	0.25000
3	0.25000	0.50000	0.25000
4	0.25000	0.25000	0.50000
5	0.66667	0.16667	0.16667
6	0.16667	0.66667	0.16667
7	0.16667	0.16667	0.66667
8	1.00000	0.00000	0.00000
9	0.75000	0.25000	0.00000
10	0.50000	0.50000	0.00000
11	0.25000	0.75000	0.00000
12	0.00000	1.00000	0.00000
13	0.00000	0.75000	0.25000
14	0.00000	0.50000	0.50000
15	0.00000	0.25000	0.75000
16	0.00000	0.00000	1.00000
17	0.25000	0.00000	0.75000
18	0.50000	0.00000	0.50000
19	0.75000	0.00000	0.25000

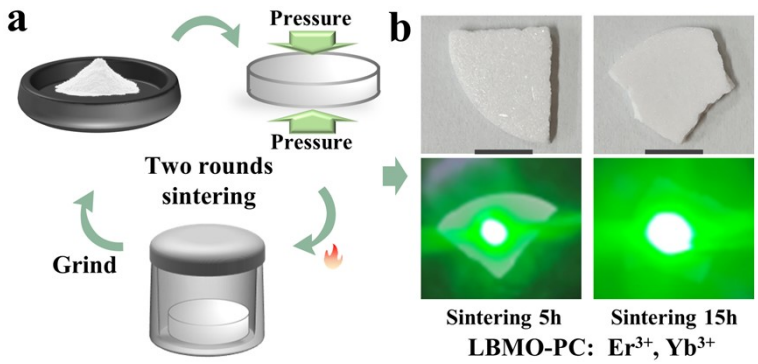

Figure S2. Schematic diagram of solid state sintering of LBMO-PC: Er^{3+}, Yb^{3+}(a), photos of the sintered LBMO-PC: Er^{3+}, Yb^{3+}(b).

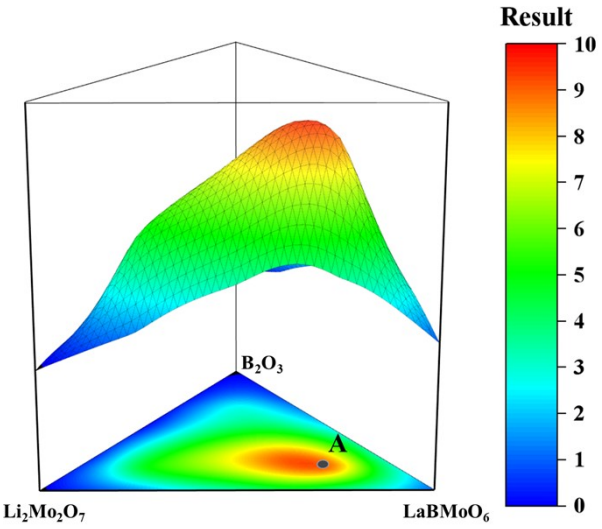

Figure S3. 3D plots of response surface corresponding to mixing design.

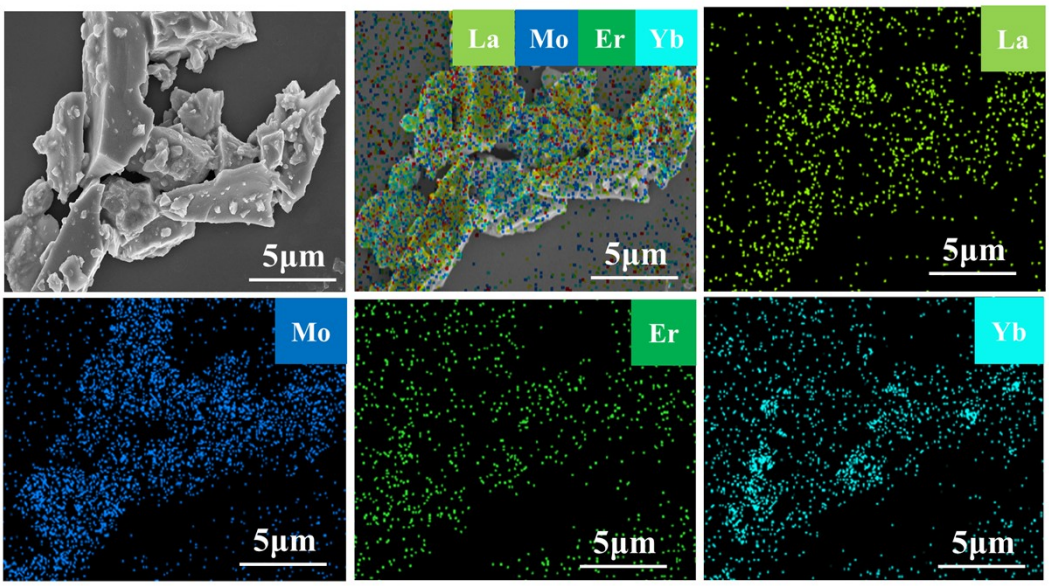

Figure S4. SEM image and EDS element mapping of LBMO-PC: Er^{3+}, Yb^{3+}.

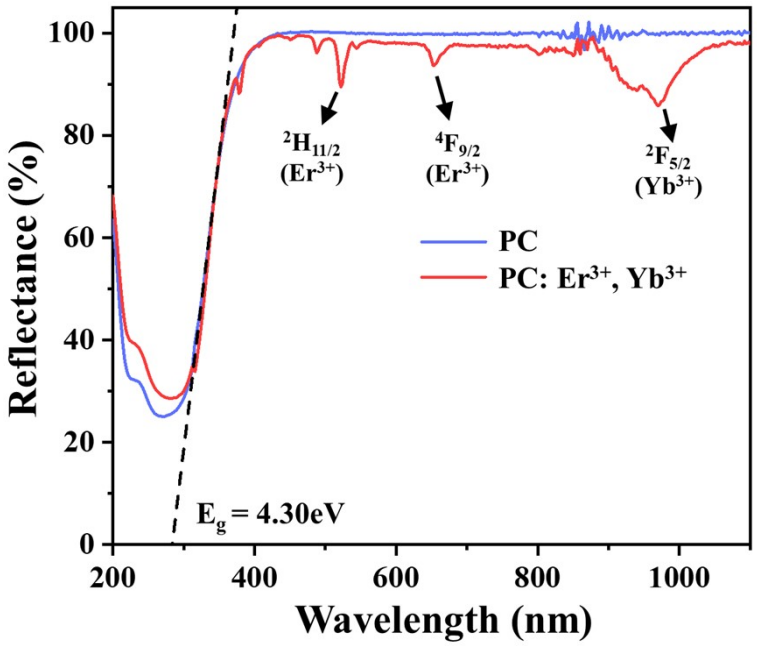

Figure S5. Diffuse reflection spectra of LBMO-PC and LBMO-PC: Er^{3+}, Yb^{3+} samples.

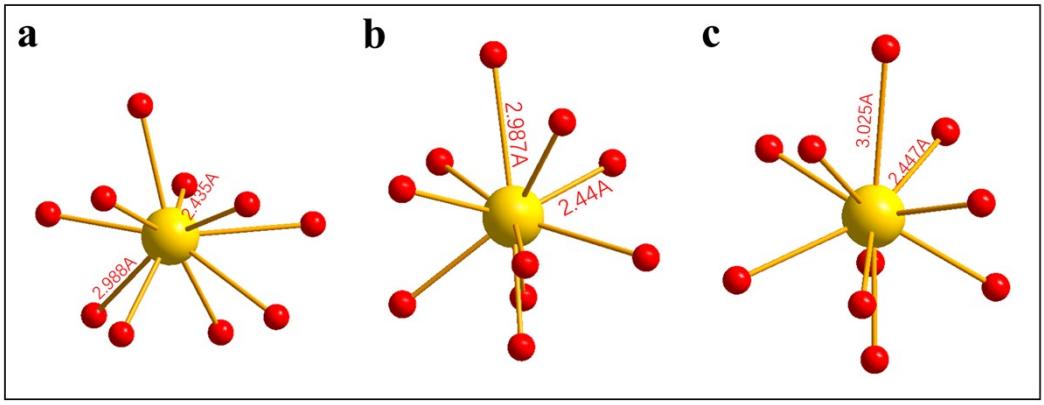

Figure S6. Ball-and-stick model of La^{3+} sites with different coordination modes.

Table S2. The total energy of Er^{3+} and Yb^{3+} occupying different cationic site in LBMO lattice

Dopants	La1 site	La2 site	La3 site	Pure LBMO lattice
Er^{3+}	-455.46 eV	-455.35 eV	-455.46 eV	-456.29
Yb^{3+}	-449.36 eV	-449.34 eV	-449.35 eV	

Table S3. The ICP-AES measurement result of LBMO-SC: 1% Er^{3+}, 20% Yb^{3+},

Element	Elemental mass fraction in sample
La	38.9003%
Er	0.0749%
Yb	0.4337%
B	2.6430%
Mo	27.7912%

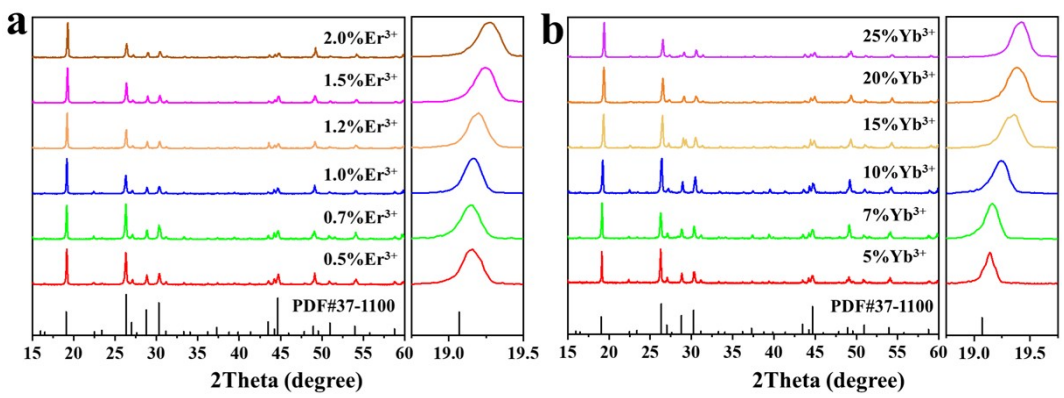

Figure S7. XRD patterns of LBMO-SC: x%Er^{3+}, 7%Yb^{3+} (a) and LBMO-SC:1%Er^{3+}, y%Yb^{3+} (b).

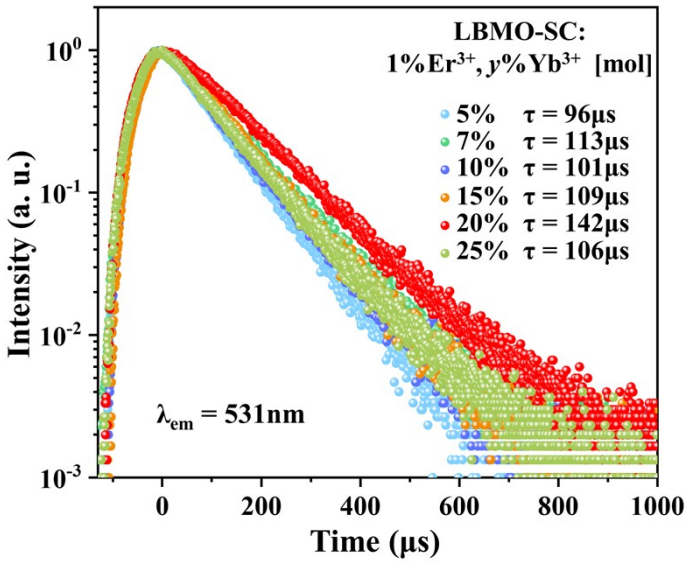

Figure S8. Luminescence decay curves of LBMO-SC: 1% Er^{3+}, *y*% Yb^{3+}.

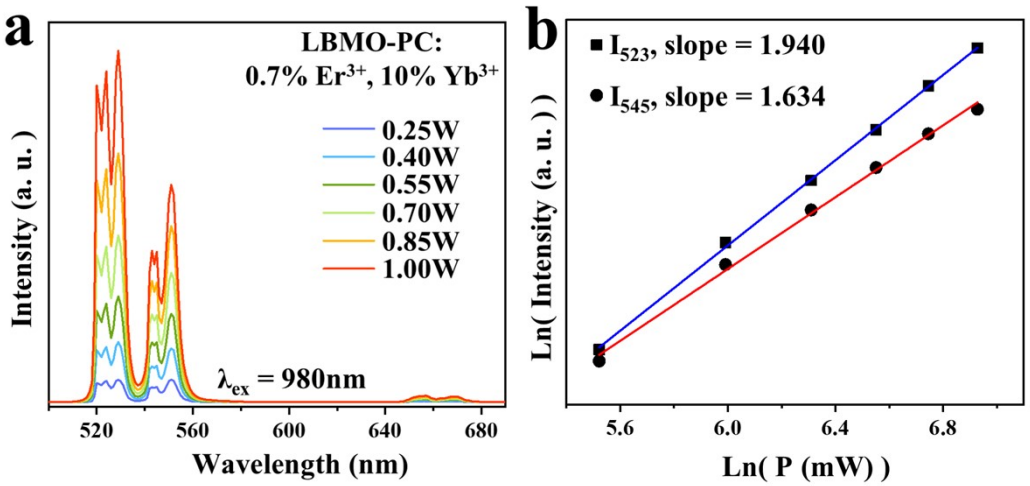

Figure S9. Pumping power-dependent up-conversion emission spectra (a) and plot of log(I) *vs.* log(P) diagram (b) of LBMO-PC: 0.7%Er^{3+}, 10%Yb^{3+}.

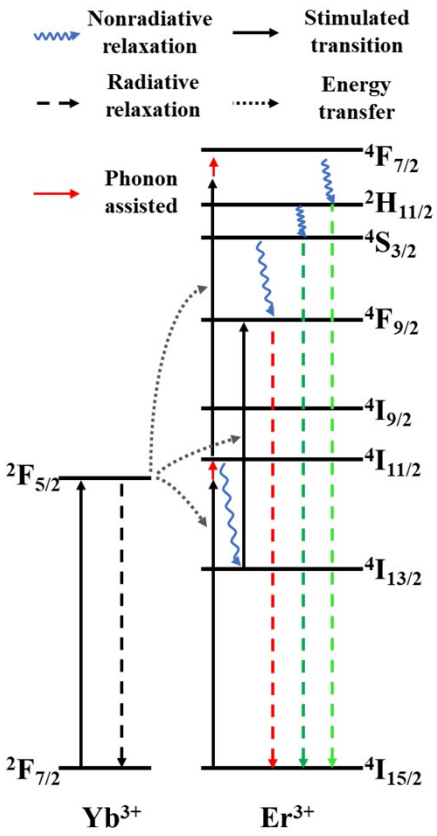

Figure S10. Energy levels schematic diagram of Er^{3+} and Yb^{3+} and simple energy transfer process between them.

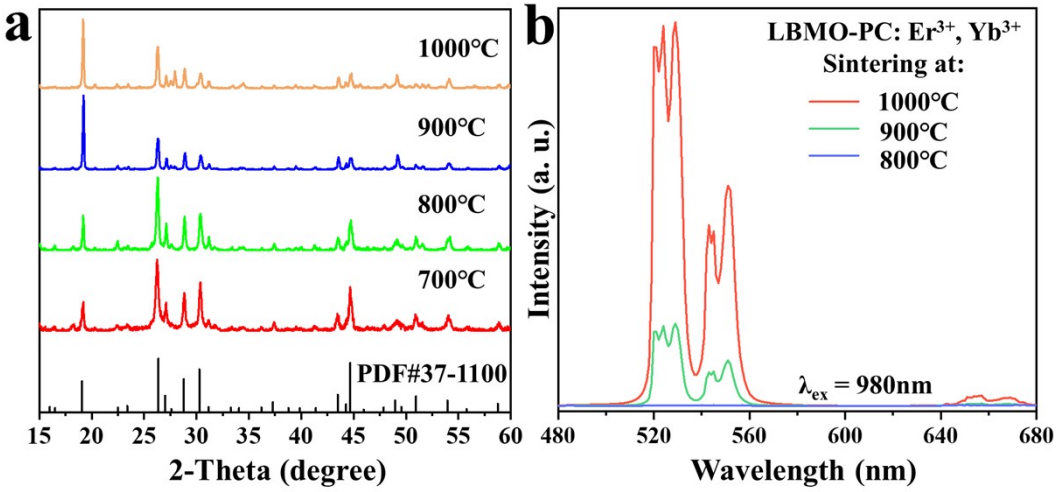

Figure S11. The PXRD patterns (a) and UC spectra (b) of LBMO-PC: 0.7%Er^{3+}, 10%Yb^{3+} powders sintered at 1000 ºC, 900 ºC and 800 ºC.

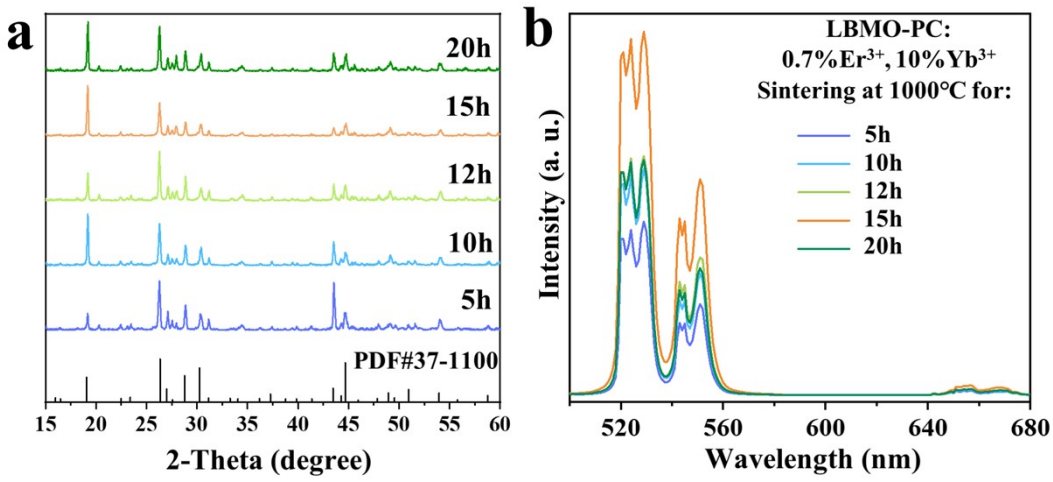

Figure S12. PXRD patterns (a) and UC spectra (b) of LBMO-PC: Er^{3+}, Yb^{3+} powders sintered at 1000 ºC for different time.

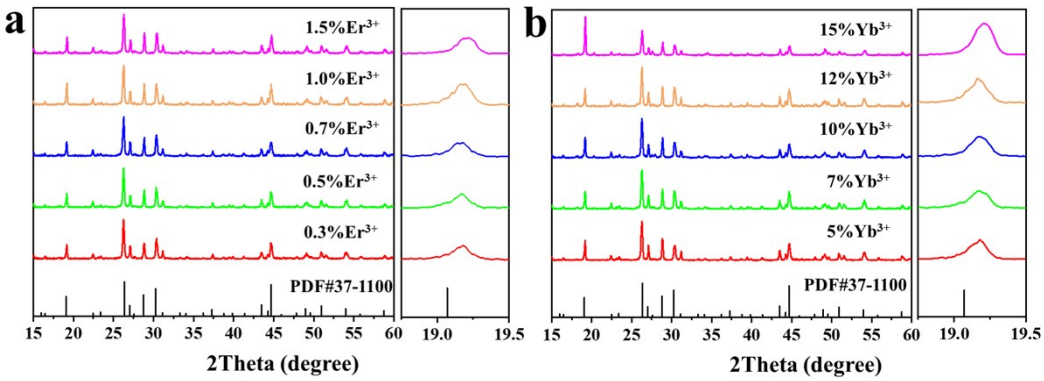

Figure S13. PXRD patterns of LBMO-PC: *x*% Er^{3+}, 10%Yb^{3+} (a) and LBMO-PC: 0.7% Er^{3+}, *y*% Yb^{3+} (b).

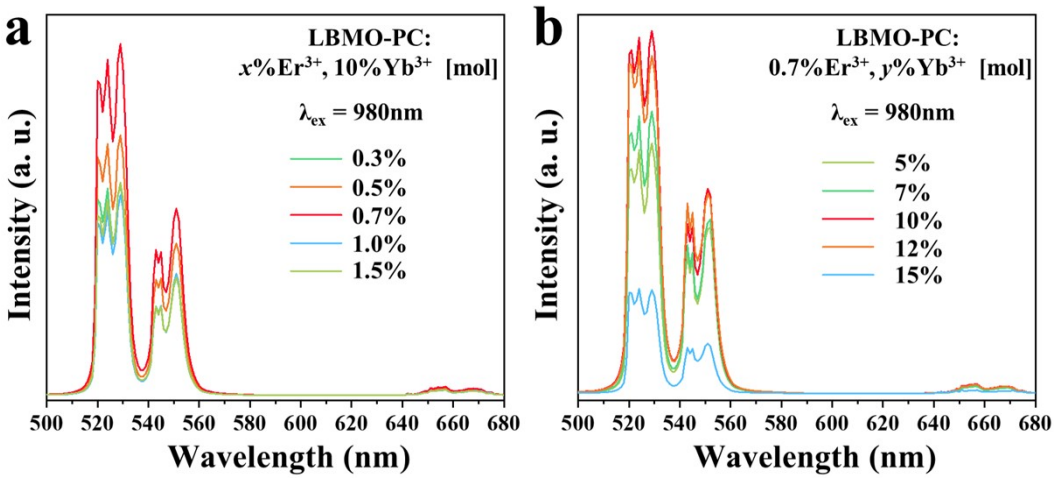

Figure S14. UC luminescence spectra of LBMO-PC: *x*% Er^{3+}, 7% Yb^{3+} samples (a) and LBMO-PC: 1% Er^{3+}, *y*% Yb^{3+} samples(b).

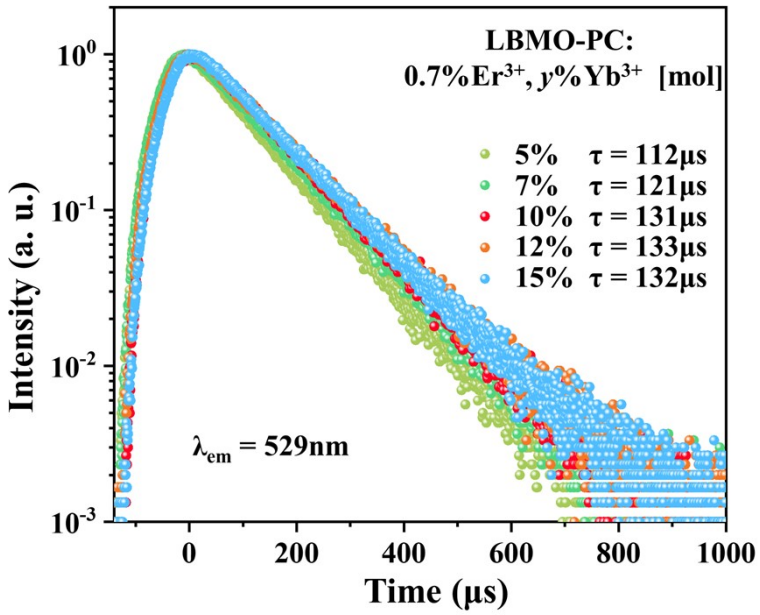

Figure S15. Luminescence decay curves of LBMO-PC: 0.7% Er^{3+}, *y*% Yb^{3+}.

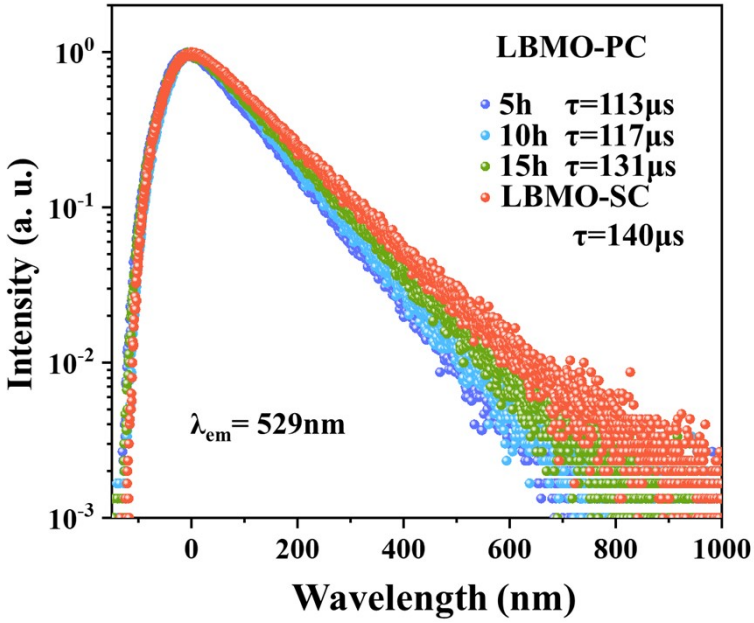

Figure S16. Luminescence decay curves of LBMO-SC: 1% Er^{3+}, 20% Yb^{3+} and LBMO-PC: 0.7% Er^{3+}, 10% Yb^{3+} sintered at 1000 °C for different time.

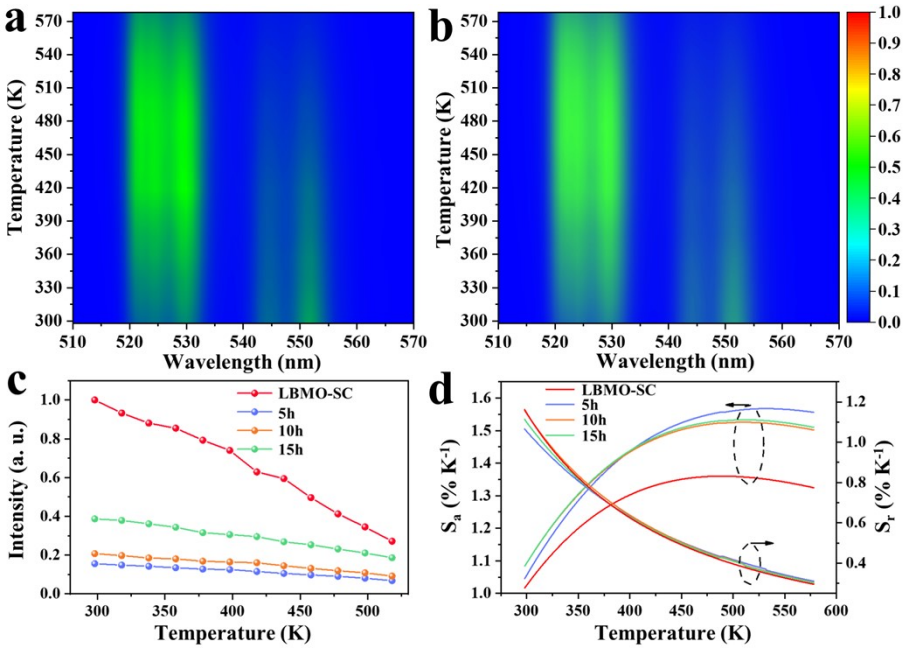

Figure S17. Flame diagram of the UC luminescence of LBMO-PC: 0.7% Er^{3+}, 10% Yb^{3+} samples sintered at 1000 °C for 5h (a) and 10h (b). Evolution of the integrated luminescence intensity of the $^4S_{3/2} \rightarrow {}^4I_{15/2}$ transition versus temperature (c) and temperature dependent S_a and S_r (d) of LBMO-SC: 1% Er^{3+}, 20% Yb^{3+} and LBMO-PC: 0.7% Er^{3+}, 10% Yb^{3+} sintered at 1000 °C for different time.

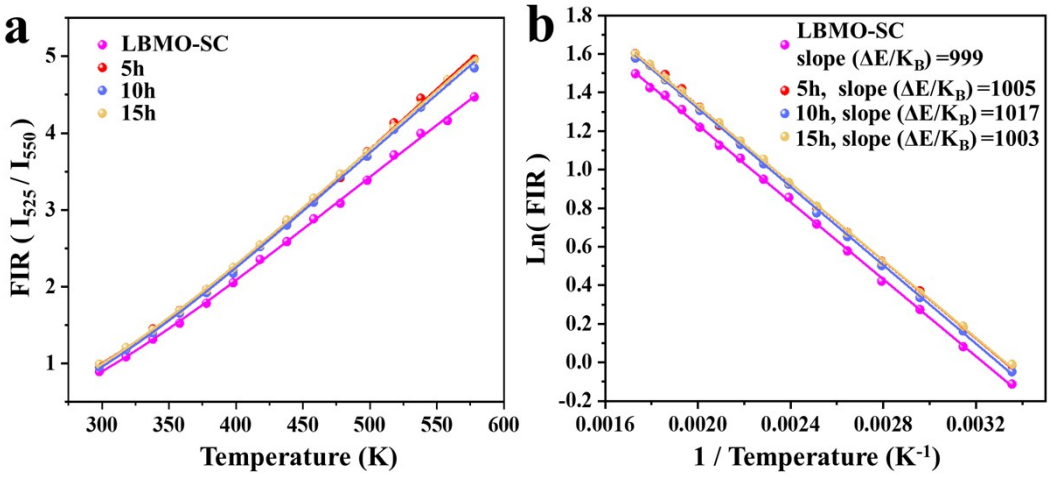

Figure S18. FIR (a) and evolution of the natural logarithm of FIR versus the reciprocal of temperature (b) of LBMO-SC: 1%Er^{3+}, 20%Yb^{3+} and LBMO-PC: 0.7%Er^{3+}, 10%Yb^{3+} sintering at 1000 °C for 5h, 10h and 15h.

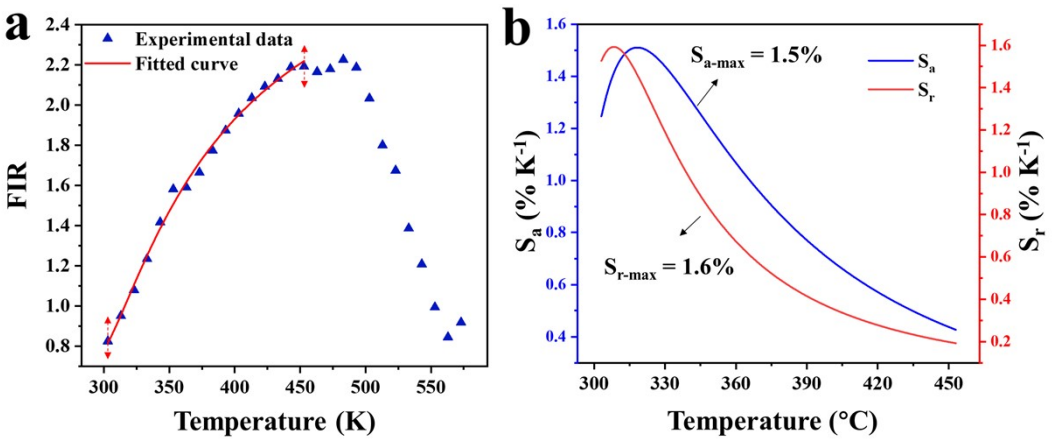

Figure S19. FIR (a) and temperature sensitivity coefficient S_a and S_r (b) of the temperature sensing device with LBMO-SC: 1% Er^{3+}, 20% Yb^{3+} as sensing media.